NIR emissive light-harvesting systems through passivation perovskite and sequential energy transfer for third-level fingerprint imaging

Kaipeng Zhong[a], Siyu Lu*[b], Wenting Guo[a], Junxia Su[a], Shihao Sun[a], Jun Hai*[a], Baodui Wang*[,a]

[a]State Key Laboratory of Applied Organic Chemistry and Key Laboratory of Nonferrous Metal Chemistry and Resources Utilization of Gansu Province, Lanzhou University, Gansu, Lanzhou, 730000, China.

[b]Green Catalysis Center, and College of Chemistry, Zhengzhou University, Zhengzhou 450000, People's Republic of China.

1. Experimental section

1.1 Materials and physical methods

All the commercial materials and reagents were purchased from Energy Chemical or Aladdin Reagents and used directly as received. All other reagents and solvents were commercially available at analytical grade and were used without further purification. Field-emission scanning electron microscope (FE-SEM, FEI, Sirion 200), transmission electron microscope (TEM, Tecna i-G2-F30 (FEI)), X-ray powder diffraction (XRD, AXS D8-Advanced diffractometer), UV-vis absorbance measurements were recorded on Shimadzu UV-1750. Photoluminescence (PL) spectra were acquired on an Edinburgh Instruments FLS920 fluorescence spectrometer. For the measurement of PL lifetime, the used excitation wavelength (λ_{ex}) was 360 nm and the maximum emission wavelength (λ_{em}) was 550 nm. The average lifetime (Ave. τ) is calculated according to $\tau = \tau_1 \cdot I_1 + \tau_2 \cdot I_2 + \tau_3 \cdot I_3$ (τ_i is the lifetime; I_i is the relative intensity).[1] Single-crystal X-ray diffraction (SC-XRD) data was collected at 291.4 K, using a Supernova (Agilent Technologies Co., Ltd. Poland). ^{1}H-NMR spectrums were gathered on a JEOL ESC 400 M instrument. Chemical shifts are reported in ppm downfield from tetramethylsilane (TMS, δ scale with solvent resonances as internal standards). Mass spectra were performed on a Bruker Esquire 3000 plus mass spectrometer (Bruker-Franzen Analytik GmbH Bremen, Germany) equipped with ESI interface and ion trap analyzer. FT-IR spectra were performed on a Nicolet FT-170SX spectrometer. Melting points were measured on an X-4 digital melting-point apparatus (uncorrected). Fluorescence microscopic images were obtained with a microscope (Zeiss).

1.2 Synthesis and assembly performance

In this system, the -COOH passivated the surface defects of $MAPbBr_3$ QDs, thereby enhancing the PLQY of QDs.[2a, 2b] NiB as a NIR emissive dye was inserted into the metal supramolecular organic framework $MAPbBr_3$@Zn(II)TCP⊃EYB, and NIR emission was achieved through sequential fluorescence resonance energy transfer (FRET). In the formed assembly unit, the compounds TCP and EYB were

synthesized according to the literature (Schemes S1 and S2). A one-dimensional (1D) Zn(II)TCP coordination polymer was formed by Zn^{2+} ion coordination with carboxyl of TCP. EYB as a guest molecular was self-assembled with Zn(II)TCP coordination polymer through host-guest interaction to form Zn(II)TCP⊃EYB. Interestingly, the resulting Zn(II)TCP⊃EYB contains uncoordinated carboxyl groups, which could further coordinate with Pb^{2+} ions to form Pb(II)/Zn(II)TCP⊃EYB. To achieve targeted imaging of LFPs, the resulting Pb(II)/Zn(II)TCP⊃EYB further modified with lysozyme-binding aptamer (denoted as LBA) to form LBA-Pb(II)/Zn(II)TCP⊃EYB.[2] In the presence of CH_3NH_3Br, the $MAPbBr_3$ QDs was in-situ growth into the metal supramolecular organic framework LBA-Pb(II)/Zn(II)TCP⊃EYB. Since a large number of $MAPbBr_3$ QDs donors were in situ growth in the hydrophobic Zn(II)TCP⊃EYB assembly, the first step FRET process from $MAPbBr_3$ QDs to nearby receptor EYB was efficiently achieved. Then, as the NiB entered the pores of LBA-$MAPbBr_3$@Zn(II)TCP⊃EYB, an effective second-step FRET process from EYB to the nearby receptor NiB was realized.

2. Synthesis and characterizations of compounds **1**, **2**, **3**, **4**, **5**, **6**, **TCP, EYB**

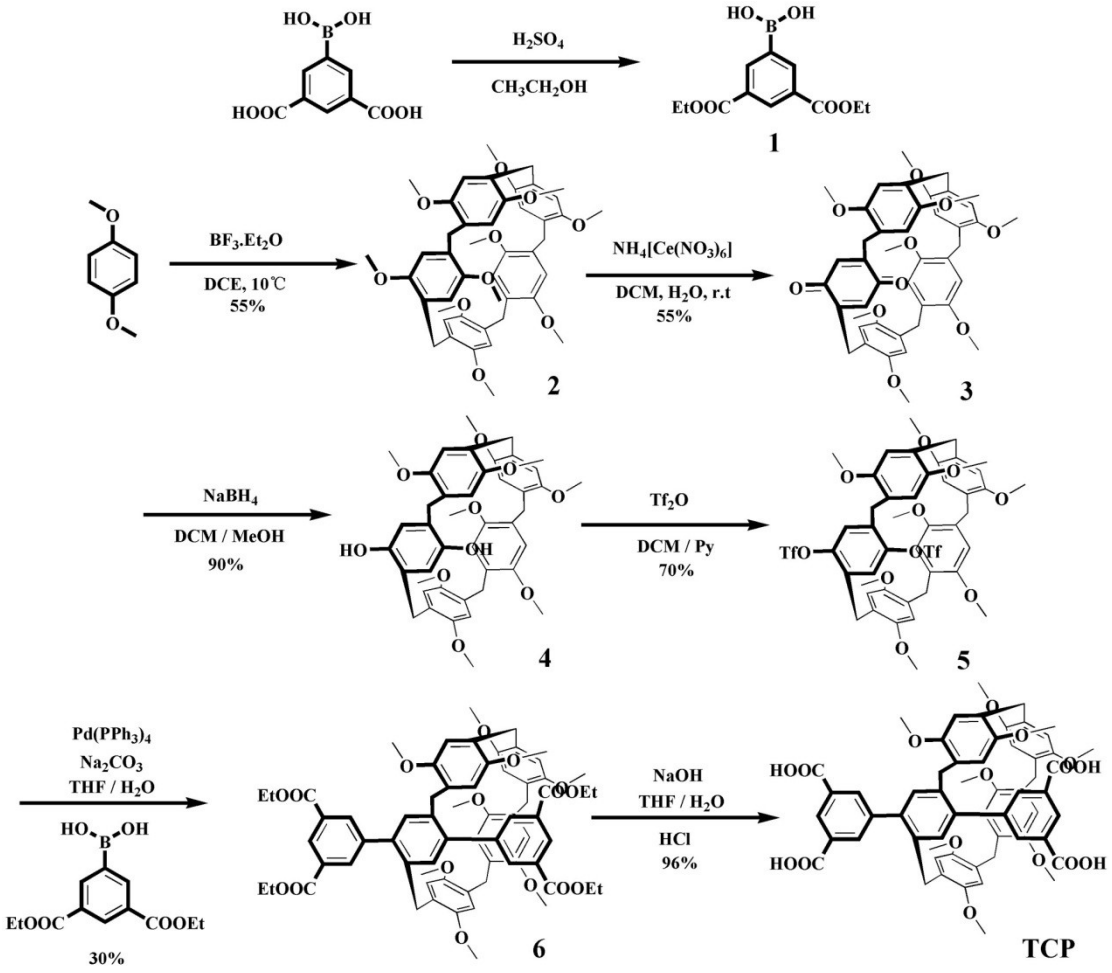

Scheme S1 Synthesis routes to the target compounds.

Synthesis of 1: 3, 5-Dicarboxybenzeneboronic acid (2.1 g, 10.0 mmol) was dissolved in dry ethanol (100 mL) in a 250 mL round-bottom flask, and added dropwise over 1 ml H_2SO_4. After the reaction mixture was stirring at 80 °C for 12 h and cooled to room temperature. The solvent is concentrated to 20ml and 100ml of water was added for suction filtration to obtain a white solid and dried to obtain **1**. ^{1}H NMR (400 MHz, $CDCl_3$, 298 K): δ 8.60 (d, J = 1.8 Hz, 2H), 8.46 (s, 1H), 4.32 (q, J = 7.1 Hz, 4H), 1.31 (t, J = 7.1 Hz, 6H).

Synthesis of 2: 1,4-Dimethoxybenzene **(**7 g, 50 mmol) and $(CH_2O)_n$ (4.5 g, 150 mmol) were dissolved in dry dichloroethane (500 mL) in a 1000 mL round-bottom flask. After the reaction mixture was stirring at 0 °C for 30 minutes, $BF_3{\cdot}OEt_2$ (7 mL, 66 mmol) was added into the flask carefully. When the starting material was fully

consumed (ca. 30 minutes) as monitored by TLC every 3 minutes, the reaction was quenched with $NaHCO_3$ aqueous solution and extracted with DCM 3 times. The organic layers were combined and dried over magnesium sulfate, then concentrated under vacuum after filtration. The crude product was further purified by silica gel column chromatography (petroleum ether/dichloromethane, 1: 2 v/v as the eluent) to give **2** as a white solid (3.75 g, 55%). ^{1}H NMR (400 MHz, $CDCl_3$, 298 K): δ 6.78 (s, 10H), 3.77 (s, 10H), 3.66 (s, 30H).

Synthesis of 3: Compound **2** (3 g, 4 mmol) was dissolved in DCM (200 mL) under stirring at room temperature in a 500 mL round-bottom flask. Then a solution of $(NH_4)_2[Ce(NO_3)_6]$ (4.38 g, 8 mmol) was added into the reaction solution dropwise. After stirring for 40 minutes, the reaction was stopped and the mixture was extracted with DCM and washed with NaCl aqueous solution 3 times. The organic extracts were combined and dried over magnesium sulfate. Then, after filtering off the solid, the filtrate was concentrated under vacuum and further purified by silica gel column chromatography (petroleum ether/dichloromethane, 1: 1, v/v as the eluent) to give **3** as a red powder (1.6 g, 55%). ^{1}H NMR (400 MHz, $CDCl_3$, 298 K): δ 6.87 (d, 2H), 6.82 (d, 4H), 6.67 (d, 4H), 3.77 (s, 6H), 3.73 (m, 18H), 3.65 (s, 6H), 3.58 (s, 4H). ESI-MS m/z: [**3** + H^+] Calcd for $C_{43}H_{45}O_{10}$, 721.30; Found 721.2923.

Synthesis of 4: Compound **3** (1.4 g, 2 mmol) was dissolved in DCM (20 mL) in a 50 mL round-bottom flask. Then a solution of Na_2BH_4 aqueous solution (106 mL, 2 M) was added into the above solution dropwise under vigorous stirring. After 30 minutes, the reaction was stopped and the resulting mixture was extracted with DCM and washed with NaCl aqueous solution for 3 times. The organic layer was dried over magnesium sulfate and then concentrated under a vacuum to give a white powder (1.4 g, 97%). ^{1}H NMR (400 MHz, CDCl3, 298 K): δ 7.17 (d, 2H), 6.91 (d, 2H), 6.83 (s, 2H), 6.82 (s, 2H), 6.60 (d, 4H), 3.85 (m, 8H), 3.76 (d, 10H), 3.73 (s, 6H), 3.67 (d, 10H).

Synthesis of 5: Trifluoromethanesulfonic anhydride (4 mL) was added dropwise to a mixture of **4** (1.4 g, 2 mmol) and pyridine (dry, 2 mL) in DCM (dry, 20 mL) at 0 °C.

Then, the reaction mixture was allowed to stir at room temperature for 12 hours. The reaction was stopped and the resulting mixture was extracted with DCM and washed with NaCl aqueous solution for 3 times. The organic extracts were concentrated under vacuum and further purified by silica gel column chromatography (petroleum ether/ ethyl acetate, 50: 1, v/v as the eluent) to give a white powder (1.38 g, 70%). ^{1}H NMR (400 MHz, $CDCl_3$, 298 K): δ 7.34 (m, 2H), 6.82 (s, 2H), 6.79 (s, 2H), 6.78 (s, 2H), 6.70 (s, 2H), 3.85 (s, 4H), 3.80 (s, 6H), 3.73 (s, 6H), 3.70 (s, 6H), 3.67 (s, 6H), 3.63 (s, 6H).

Synthesis of 6: A mixture of pillar[5]arene **5** (1.10 g, 1.0 mmol), [3,5-Bis(ethoxycarbonyl)phenyl]boronic Acid (900.0 mg, 5.0 mmol), Na_2CO_3 (650.0 mg， 5.0 mmol) and $Pd(PPh_3)_4$ (300.0 mg, 0.26 mmol) in a mixed solvent of THF and H_2O (60 ml, 5:1, *v/v*) was heated under N_2 at 80 ºC for 36 h, then poured into water (100 mL), and extracted with $CHCl_3$ (3 × 100 mL). The combined organic phases were concentrated to result in a residue which was subjected to column chromatography (petroleum ether/ethyl acetate, 20:1, *v/v*) to afford **6** as a white solid (0.55 g, 51%). ^{1}H NMR (400 MHz, $CDCl_3$, 298 K) δ 8.69 (t, *J* = 1.6 Hz, 2H), 8.16 (s, 4H), 7.39 (s, 2H), 6.85 (s, 2H), 6.63 (d, *J* = 65.5 Hz, 4H), 5.59 (s, 2H), 4.41 (q, *J* = 7.1 Hz, 8H), 3.93 (d, *J* = 13.4 Hz, 2H), 3.81 (t, *J* = 6.7 Hz, 4H), 3.72 – 3.59 (m, 18H), 3.46 (s, 4H), 3.30 (s, 6H), 1.41 (t, *J* = 7.1 Hz, 12H). ESI-MS m/z: [**6** + H^+] Calcd for $C_{67}H_{71}O_{16}$, 1131.47; Found 1131.4760.

Synthesis of TCP [3]**:** A mixture of pillar[5]arene **6** (1.07 g, 1.0 mmol) and NaOH (4.0 g, 100.0 mmol) in a mixed solvent of THF and H_2O (200 ml, 1:1, *v/v*) was heated at 50 ºC for 24 h, poured into an aqueous HCl solution (1.0 M, 300 mL), and extracted with trichloromethane (3 × 100 mL). The combined extracts were dried over anhydrous Na_2SO_4 and concentrated to result in a residue to afford **TCP** as a white solid (1.0 g, 96%). ^{1}H NMR (400 MHz,) δ 8.50 (s, 2H), 8.00 (d, *J* = 1.2 Hz, 4H), 7.33 (s, 2H), 6.76 (s, 2H), 6.69 (s, 2H), 6.29 (s, 2H), 5.87 (s, 2H), 3.68 (d, 24H), 3.34 (s, 4H), 3.14 (s, 6H).

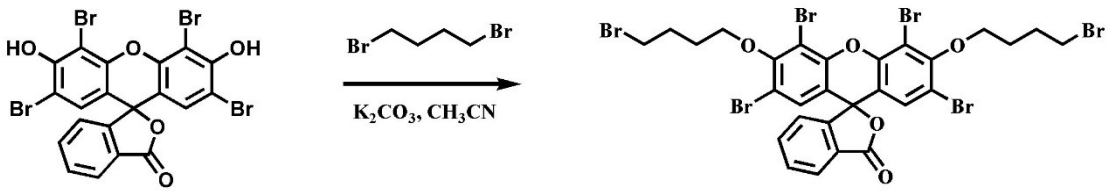

EYB

Scheme S2. Synthesis of compound **EYB**.

Synthesis of EYB: A mixture of Eosin Y (1.30 g, 2.0 mmol), K_2CO_3 (1.38 g, 10 mmol), 1,4-dibormodecane (2.40 g, 8 mmol) and acetonitrile (80.0 mL) were added to a 250 mL round-bottom flask under nitrogen atmosphere. The reaction mixture was stirred at 80 ℃ for 24 h. After the solid was filtered off, the solvent was evaporated and the residue was dissolved in CH_2Cl_2. The crude product was purified by silica gel column chromatography using petroleum ether/ethyl acetate (V / V = 20:1) as the eluent, compound **EYB** as shiny red solid (0.92 g, yield 50%) was isolated. ^{1}H NMR (400 MHz,) δ 8.32 (d, *J* = 7.7, 1.4 Hz, 1H), 7.80 (d, *J* = 19.2, 7.6, 1.4 Hz, 2H), 7.32 – 7.26 (m, 2H), 7.10 (s, 1H), 4.14 (d, *J* = 18.0, 6.1 Hz, 4H), 3.55 (t, *J* = 6.5 Hz, 2H), 3.36 (t, *J* = 6.5 Hz, 2H), 2.26 – 2.17 (m, 2H), 2.08 (d, *J* = 8.7, 5.6 Hz, 2H), 1.86 – 1.77 (m, 2H), 1.72 (d, *J* = 5.4, 3.4 Hz, 2H).

2.2 Preparation of the crystals of Zn(II)TCP.

The crystals of Zn(II)TCP was prepared by heating a mixture of TCP (20 mg) and $Zn(NO_3)_2{\cdot}6H_2O$ (20 mg) in DMF-H_2O binary solvent (v: v =5:3) at 80°C for 24 h. The crystal was kept at 291.4 K during data collection. Using Olex2, the structure was solved with the Superflip structure solution program using Charge Flipping and refined with the ShelXL refinement package using Least Squares minimisation. Crystal Data for $C_{65}H_{65}N_2O_{20}Zn$ (*M*=1260.56 g/mol): triclinic, space group P-1 (no. 2), *a*= 12.3750(9) Å, *b*= 13.3822(8) Å, *c*= 20.4459(13) Å, *α*= 101.724(5)°, *β*= 90.576(5)°, *γ*= 109.974(6)°, *V*= 3104.2(4) Å ^{3}, *Z*= 2, *T*= 291.4(4) K, μ(MoKα)= 0.473 mm^{-1}, *Dcalc*= 1.349 g/cm^3, 20011 reflections measured (6.79°≤ 2θ ≤ 51.986°), 12174 unique (R_{int}= 0.0492, R_{sigma}= 0.1183) which were used in all calculations. The final R_1

was 0.0959 ($I > 2\sigma(I)$) and wR_2 was 0.2947.

2.3 Preparation of the $MAPbBr_3$@Zn(II)TCP⊃EYB.

A mixture of Zn(II)TCP (100 μL, 0.1 m mol), EYB (100 μL, 0.1 m mol), $PbBr_2$ (10 μL, 0.1 m mol) was added to a 7 mL centrifuge tube under vigorously stirred. Next, 10 μL CH_3NH_3Br (0.1 mmol, DMF) was slowly added dropwise to the above system to obtain $MAPbBr_3$@Zn(II)TCP⊃EYB precursors. Then, a fixed amount of precursor solution was dropped into toluene under vigorous stirring and ultrasound. After that, a yellow-red colloidal solution was formed and stored in vacuum for later use.

2.4 Synthesis of lysozyme-binding aptamer-modified LBA-$MAPbBr_3$@Zn(II)TCP⊃EYB-NiB.

The product LBA-$MAPbBr_3$@Zn(II)TCP⊃EYB-NiB was facilely synthesized through the condensation of $MAPbBr_3$@Zn(II)TCP⊃EYB-NiB and LBA-NH_2 as catalyzed by 1-(3-(dimethylamino)-propyl)-3-ethylcarbodiimide hydrochloride (EDCI). 100 μL of product Pb(II)Zn(II)TCP⊃EYB-NiB was dispersed in 100 μL ethanol, and then 2 nmol LBA-NH_2 was added and stirred at room temperature for 24 h. After the product was collected, it was washed with deionized water and then freeze-dried. Subsequently, 10 μL CH_3NH_3Br (0.1 mmol, DMF) was slowly added dropwise to the above system to obtain precursors. Then, a fixed amount of precursor solution was dropped into toluene under vigorous stirring and ultrasound to obtain LBA-$MAPbBr_3$@Zn(II)TCP⊃EYB-NiB as a yellow-red colloidal solution.

2.5 Fingerprints collection.

Volunteers were asked to run their fingers across their foreheads and then blot their fingers on the chosen surfaces that were pre-cleaned with water and dried in the air. The collected samples were aged for 12 hours before being subjected to the incubation procedure.

2.6 Latent fingerprint detection.

LBA-$MAPbBr_3$@Zn(II)TCP⊃EYB-NiB solution (30 μM, dichloromethane) is dripped on the surface of substrates printed with latent fingerprints (tinfoil, steel, glass,

resin, plastic). The latent fingerprints were incubated with the solution for the 30 s at room temperature. After this process, the excess solution was carefully removed with a micropipette, and the fingerprints were washed 3 times with dichloromethane. Then the latent fingerprints were acquired images by a Single Lens Reflex (SLR) Camera (Nikon D5100) with a common cut-off filter (JB510) under a 360 nm illumination.

2.7 Energy-transfer efficiency.

Energy-transfer efficiency (Φ_{ET}) was calculated from excitation fluorescence spectra through the equation: $\Phi_{ET} = 1 - I_{DA} / I_D$.[4]

Where I_{DA} and I_D are the fluorescence intensities of the emission of $MAPbBr_3$@Zn(II)TCP⊃EYB (donor and acceptor) and $MAPbBr_3$ (donor) respectively when excited at 360 nm. The energy-transfer efficiency (Φ_{ET}) was calculated as 74.6% in toluene, measured under the condition of [TCP] = 2×10^{-5} M, [$MAPbBr_3$] =1.25×10^{-4} M, [EYB] = 5×10^{-7} M, and λ_{ex} = 360 nm. And the second-step energy-transfer efficiency (Φ_{ET}) was calculated as 74.6% in toluene.

2.8 The PLQY can be calculated using the following formula:[5]

$$\Phi = \Phi_R \frac{\int F(\lambda_{em})}{\int F_R(\lambda_{em})} \frac{A_R(\lambda_{ex})}{A(\lambda_{ex})} \frac{n^2}{{n_R}^2}$$

where Φ is the PLQY, $\int F(\lambda_{em})$ is the integrated intensity of emission, $A(\lambda_{ex})$ is the percentage of light absorbed at the excitation wavelength, n is the refractive index, and subscript R denoted the reference data. The PLQY of $MAPbBr_3$@Zn(II)TCP⊃EYB is 34.5%, and $MAPbBr_3$@Zn(II)TCP is 5.8%, respectively. The correction factor (n^2/n_R^2) was derived from the point source, which was found to be valid for many detector geometries.[6] In short, as emission passes from a material with a high to low refractive index, the refractive angle will affect the portion of photons that could be collected, thus, correlating the calculation of PLQY with the refractive index *n*. A detailed derivation method can be found in the references.[7]

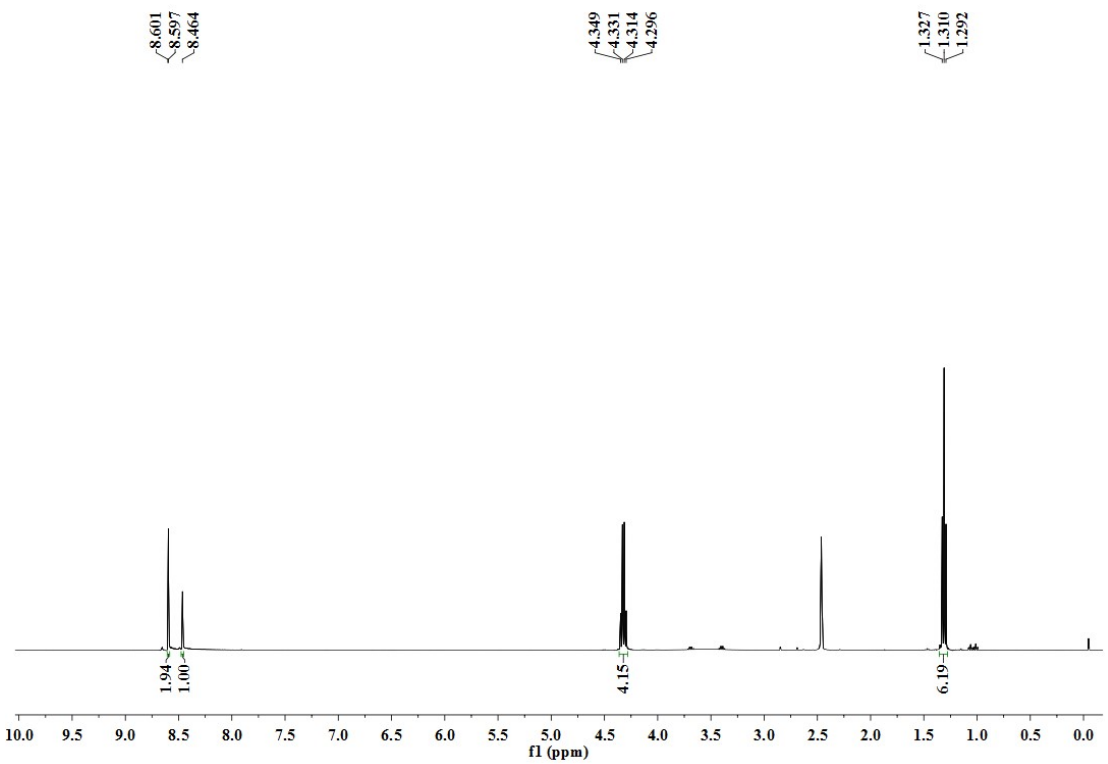

Figure. S1 ^{1}H NMR spectrum (400 MHz, $CDCl_3$, 298 K) of **1**.

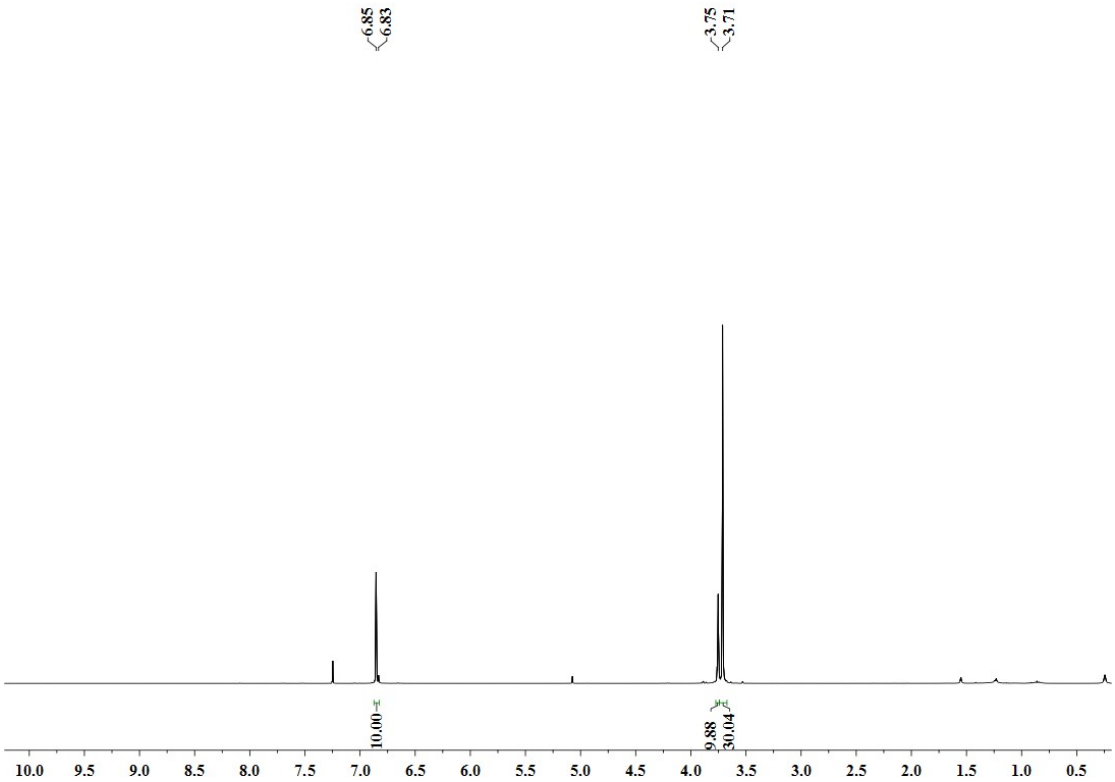

Figure. S2 ^{1}H NMR spectrum (400 MHz, $CDCl_3$, 298 K) of **2**.

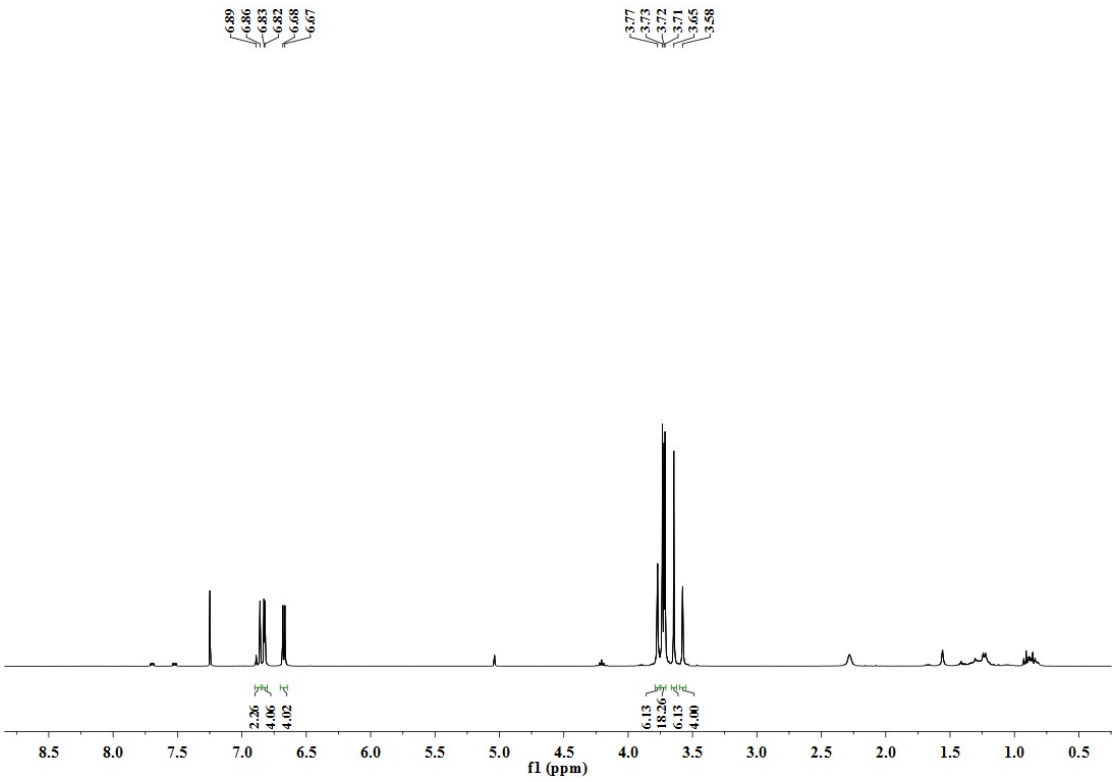

Figure. S3 ^{1}H NMR spectrum (400 MHz, $CDCl_3$, 298 K) of **3**.

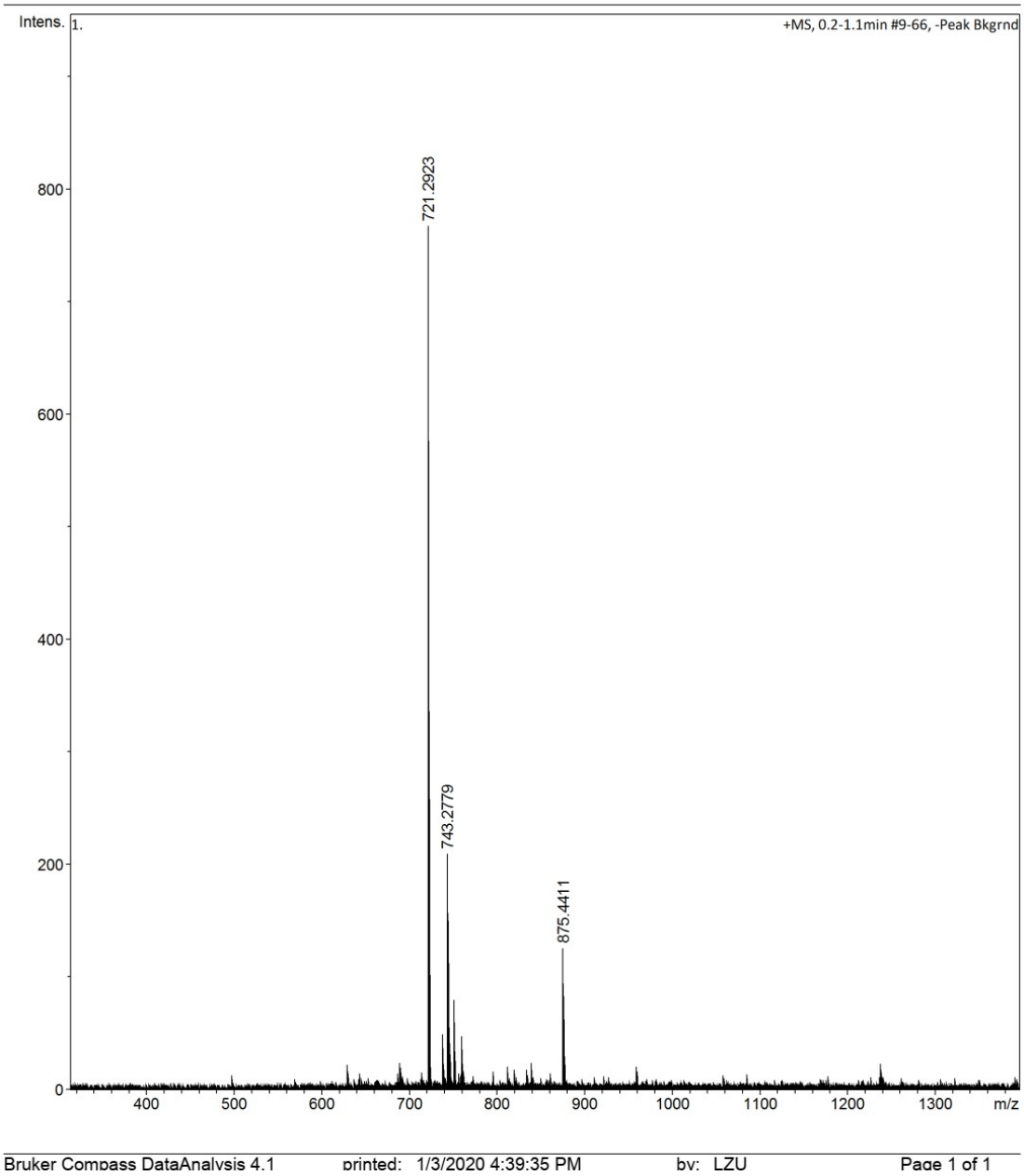

Figure. S4 MS-ES mass spectra of **3.**

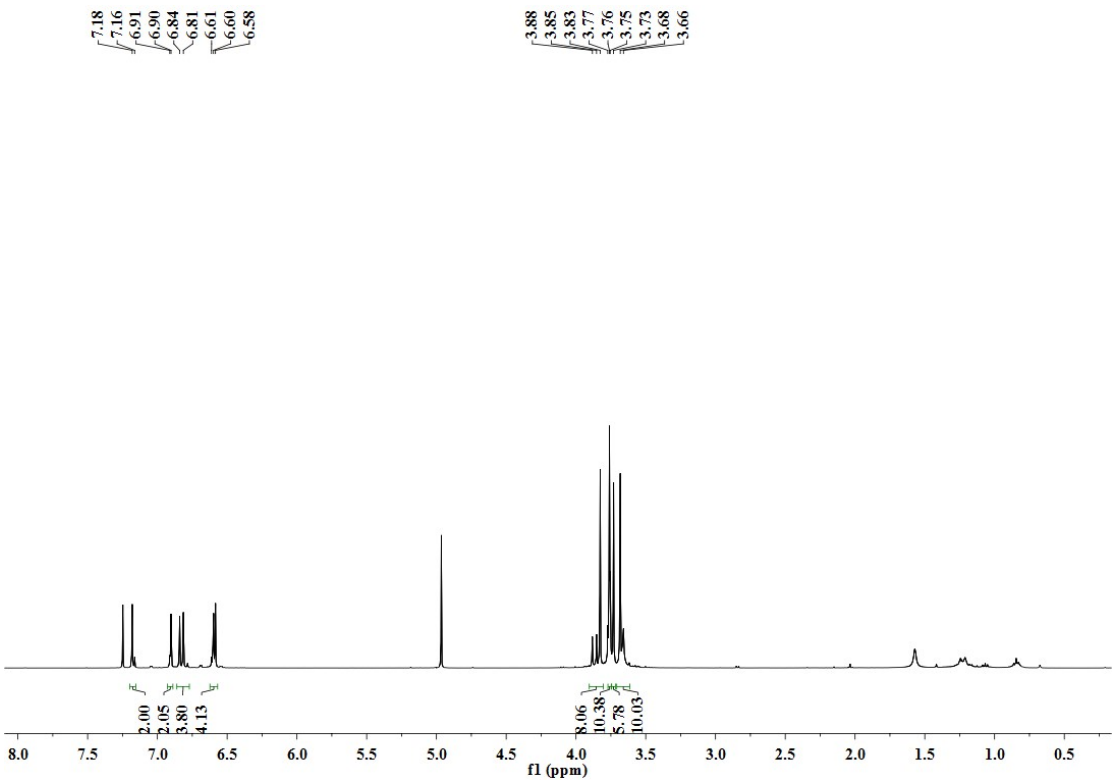

Figure. S5 ^{1}H NMR spectrum (400 MHz, $CDCl_3$, 298 K) of **4**.

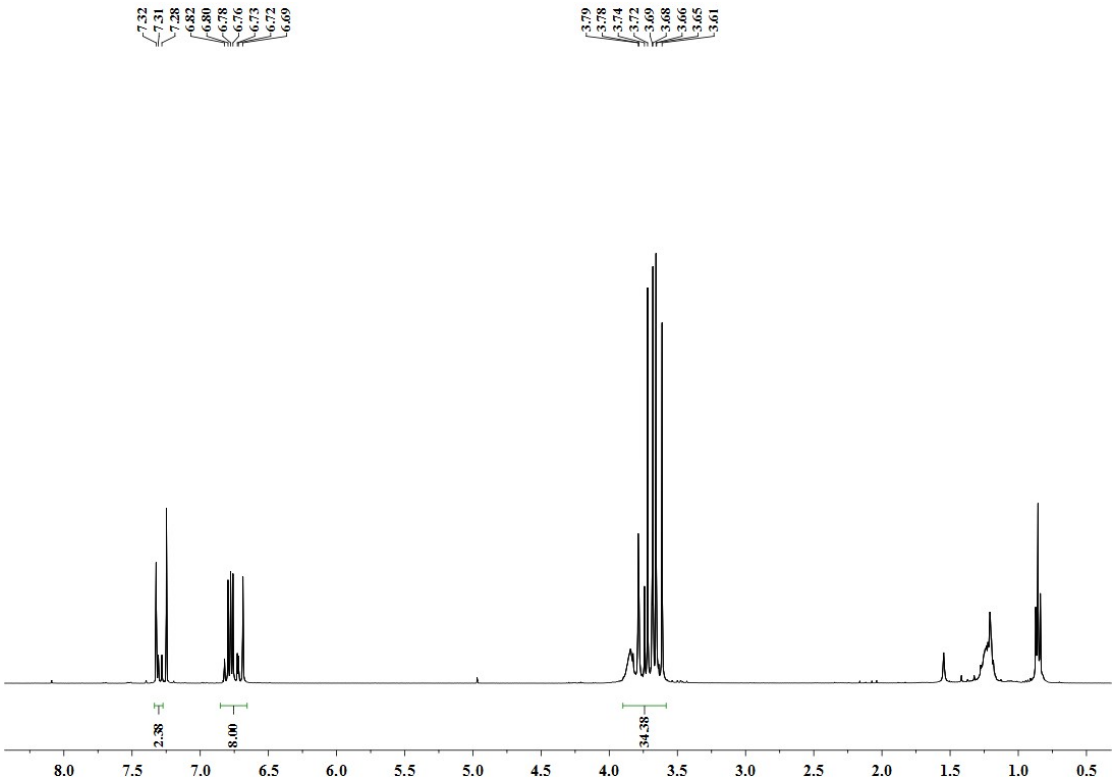

Figure. S6 ^{1}H NMR spectrum (400 MHz, $CDCl_3$, 298 K) of **5**.

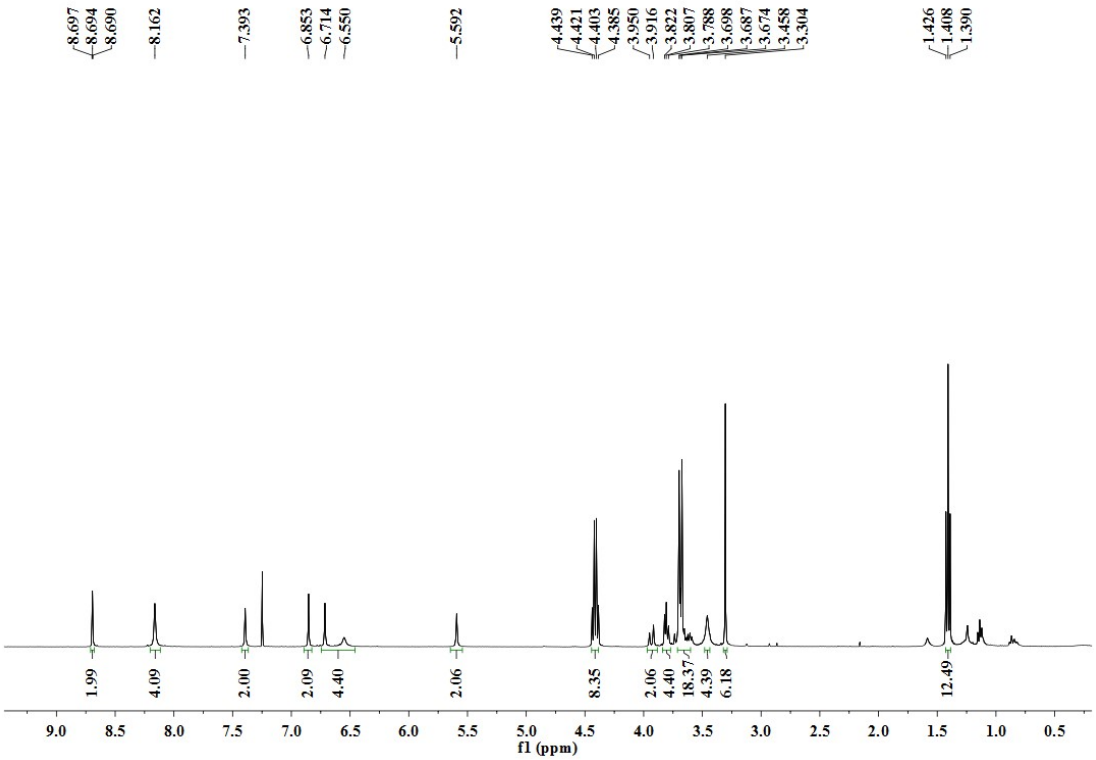

Figure. S7 ^{1}H NMR spectrum (400 MHz, $CDCl_3$, 298 K) of **6**.

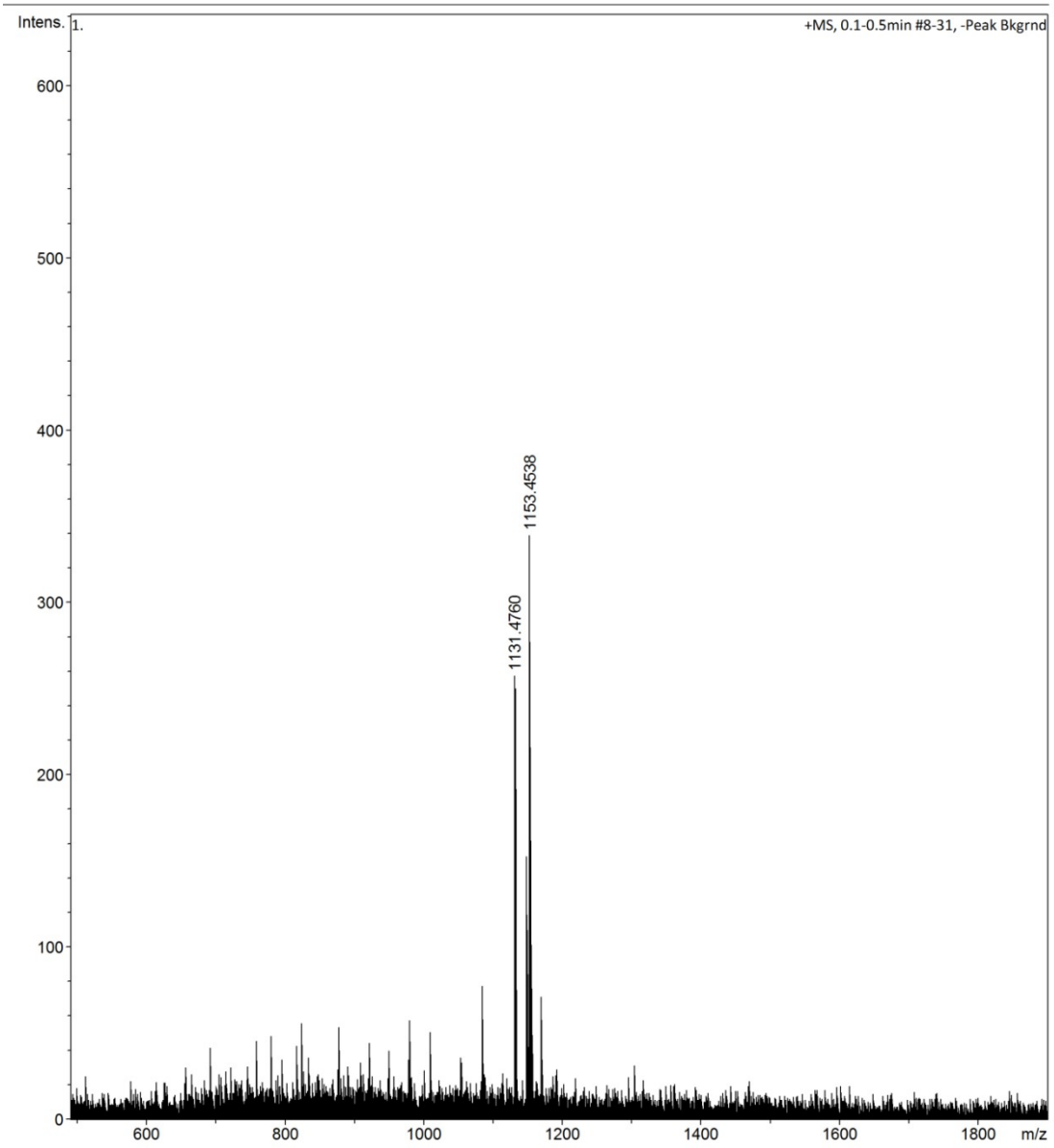

Figure. S8 ESI-MS spectrum of **6**.

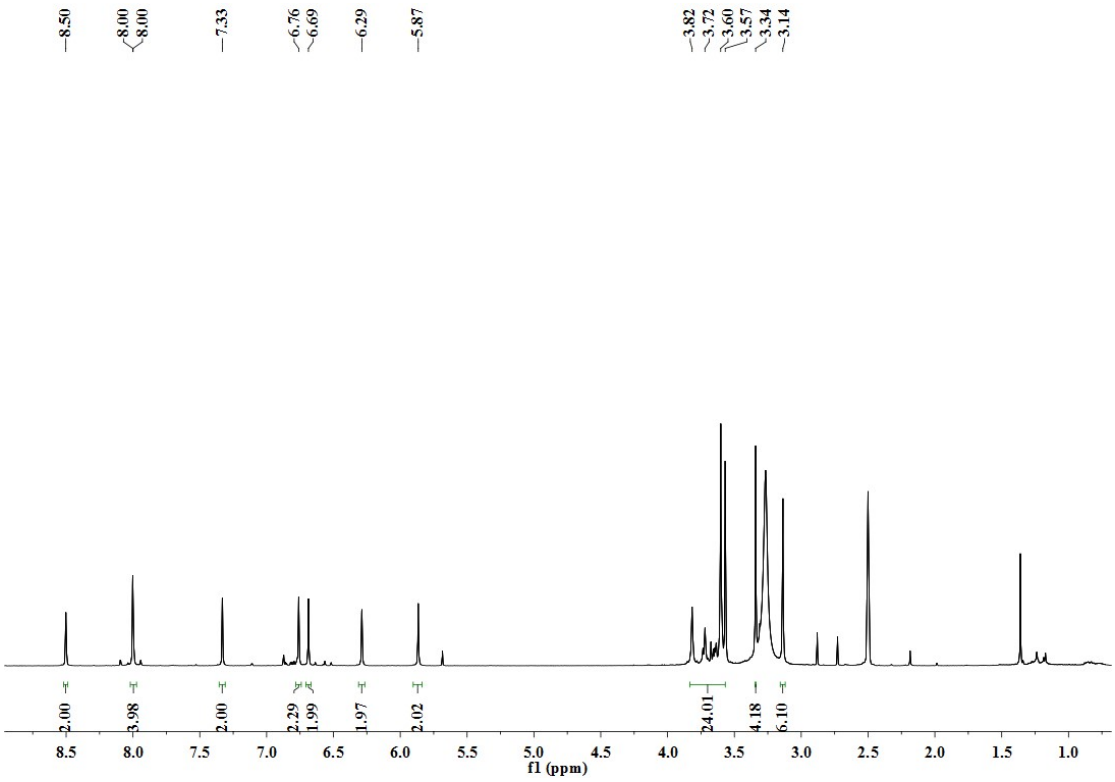

Figure. S9 [1]H NMR spectrum (400 MHz, DMSO-d_6, 298 K) of **TCP**.

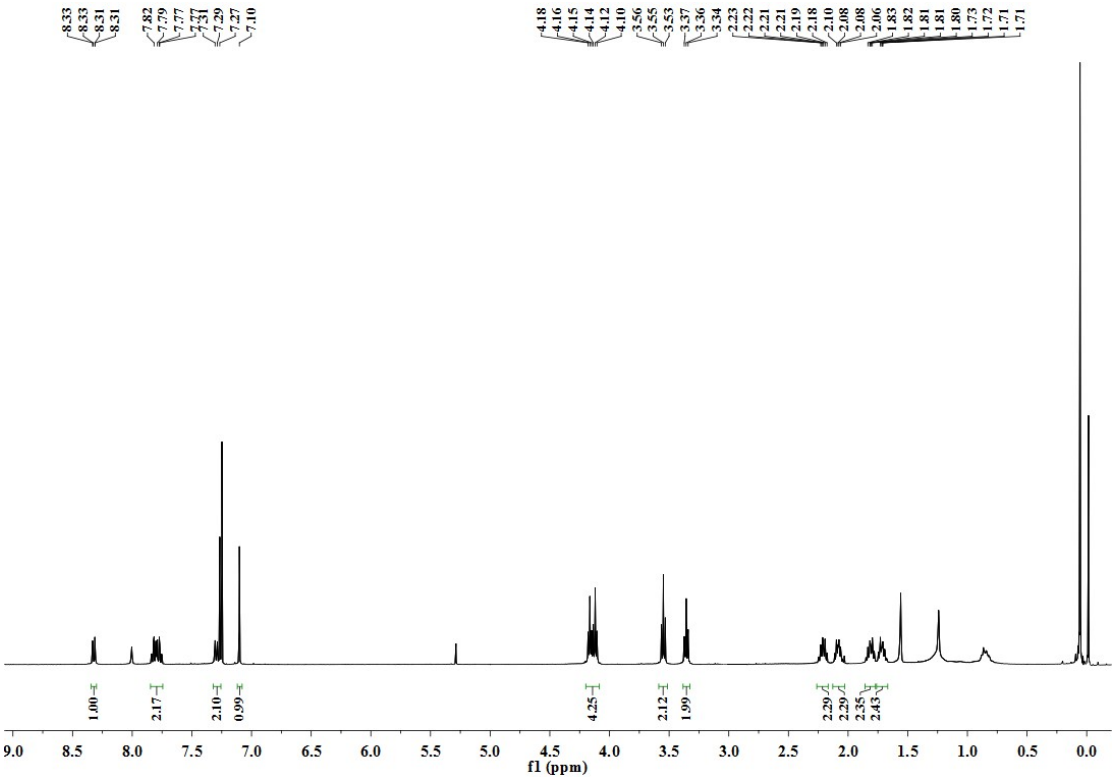

Figure S10 [1]H NMR spectrum of compound **EYB** in $CDCl_3$.

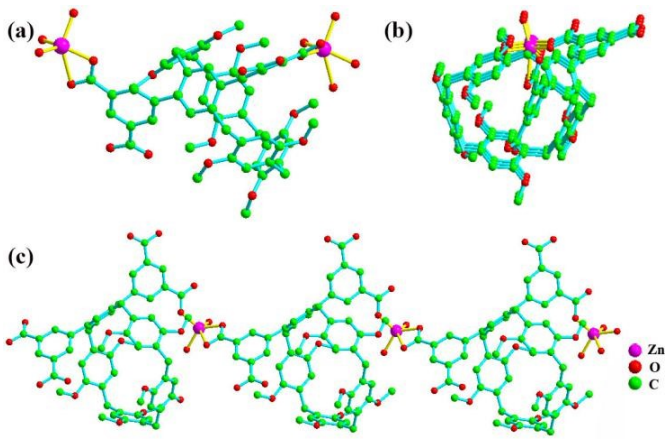

Figure S11. Crystal structure of Zn(II)TCP from (a) side, (b) top view, and (c) linear polymer.

Solvent molecules are omitted for clarity. Zn(II)TCP coordination polymer was synthesized by coordination reaction between TCP and Zn $(NO_3)_2 \cdot 6H_2O$ in DMF-H_2O double solvent at 80 ^{0}C. As shown in Figure S11, crystallographic analysis reveals that the Zn(II) coordination polymer crystallizes in the monoclinic crystal system with the space group P-1. $[Zn(TCP)(H_2O)_2(DMF)_2]_n$ exhibits 1D coordination polymer (Figure S11c). The asymmetric unit contains one Zn(II) ion, one TCP-ligand, and two coordinated water molecules, and two exposed carboxyl site groups that are not involved in the coordination.

Table S1 Crystallographic data for Zn(II)TCP.

Compound	Zn(II)TCP
Identification code	zhongkp_0327
Empirical formula	$C_{65}H_{66}N_2O_{20}Zn$
Formula weight	1260.56
Temperature/K	291.4(4)
Crystal system	triclinic
Space group	P-1
a/Å	12.3750(9)
b/Å	13.3822(8)
c/Å	20.4459(13)
α/°	101.724(5)
β/°	90.576(5)
γ/°	109.974(6)
Volume/Å^3	3104.2(4)
Z	2
ρ_{calc}g/cm^3	1.349
μ/mm^{-1}	0.473
F(000)	1320.0
Crystal size/mm^3	0.18 × 0.15 × 0.12
Radiation	MoKα (λ = 0.710)
2θ range for data collection/°	6.79 to 51.986
Index ranges	-15 ≤ h ≤ 12, -16 ≤ k ≤ 16, -25 ≤ l ≤ 23
Reflections collected	20011
Independent reflections	12174 [R_{int} = 0.0492, R_{sigma} = 0.1183]
Data/restraints/parameters	12174/6/806
Goodness-of-fit on F^2	1.021
Final R indexes [I>=2σ (I)]	R_1 = 0.0959, wR_2 = 0.2288
Final R indexes [all data]	R_1 = 0.1785, wR_2 = 0.2947
Largest diff. peak/hole / e Å^{-3}	0.71/-0.87

Table S2 Fractional Atomic Coordinates ($\times 10^4$) and Equivalent Isotropic Displacement Parameters ($Å^2 \times 10^3$) for Zn(II)TCP. U_{eq} is defined as 1/3 of of the trace of the orthogonalised U_{IJ} tensor.

Atom	*x*	*y*	*z*	U(eq)
Zn1	382.6(7)	1261.6(6)	4283.3(4)	61.3(3)
O2	1988(4)	1606(4)	4211(2)	64.5(13)
O4	-590(5)	-303(4)	3920(3)	91.4(18)
O5	2347(3)	429(3)	4730(2)	55.7(11)
O7	6376(4)	378(4)	4634(3)	71.0(14)
O6CA	3679(4)	5860(4)	4512(2)	67.9(13)
O11	-464(5)	590(4)	3145(3)	94.5(19)
O13	5395(5)	3671(4)	1161(2)	74.6(15)
O16	7753(4)	1691(5)	4325(3)	92.6(19)
O17	3980(5)	8978(4)	3045(3)	76.0(15)
O20	-1254(4)	2939(4)	2028(2)	65.1(13)
O21	78(4)	2630(4)	4283(3)	72.3(14)
O23	1696(5)	417(5)	1800(3)	87.3(17)
O9AA	1048(5)	6117(4)	1084(3)	85.5(16)
O1BA	-304(5)	6507(4)	3660(3)	87.1(17)
O2BA	5419(7)	7315(6)	1029(3)	120(3)
C31	4185(5)	2479(4)	3913(3)	44.6(14)
C34	6298(5)	4928(4)	2595(3)	39.5(13)
C0AA	5909(5)	3927(4)	2784(3)	40.1(13)
C37	6352(5)	5900(4)	3016(3)	41.4(13)
O40	1464(6)	2765(6)	-83(3)	103(2)
C42	5604(5)	3928(4)	3445(3)	40.0(13)
C43	5292(5)	2932(4)	3731(3)	42.1(13)
O46	6629(7)	8969(6)	1162(4)	127(3)
C48	3870(5)	1582(4)	4222(3)	40.7(13)
C50	2658(5)	1155(5)	4404(3)	48.0(15)
C1	6847(5)	6919(5)	2773(3)	43.4(14)
C8BA	4715(5)	1165(4)	4351(3)	43.8(14)
C6	5946(5)	5881(4)	3659(3)	41.5(13)
C8	5826(5)	1619(5)	4189(3)	42.8(14)
C7CA	4628(5)	2450(4)	1856(3)	43.6(14)
C12	4800(5)	7151(4)	3940(3)	44.3(14)
C2AA	4878(6)	7929(5)	3569(3)	49.9(15)
C15	5775(5)	2894(4)	2270(3)	44.0(14)
C18	6100(5)	2499(5)	3870(3)	47.0(14)
N20	2131(7)	4229(5)	2732(3)	75.0(19)

C7AA	-554(6)	2876(5)	1522(3)	51.9(16)
C24	5842(5)	6879(5)	4123(3)	48.4(15)
C25	5591(5)	4886(5)	3850(3)	45.5(14)
C27	7771(5)	7796(5)	3125(3)	49.2(15)
C29	6745(6)	1233(5)	4381(3)	53.3(16)
C32	3709(5)	1624(5)	2014(3)	50.9(15)
C5BA	6401(6)	7029(5)	2176(3)	51.6(15)
O36	635(6)	3910(5)	3394(4)	107(2)
C38	-1544(7)	2106(7)	2400(4)	83(2)
C39	2880(6)	7713(5)	3638(3)	54.6(17)
C0CA	-295(5)	5463(5)	1849(4)	55.6(17)
C44	3716(6)	6640(5)	4151(3)	50.7(16)
C45	7751(6)	8830(5)	2303(4)	61.0(18)
C47	8218(6)	8765(5)	2909(3)	54.2(16)
C6AA	4446(6)	2870(5)	1313(3)	56.5(17)
C9BA	3955(6)	8207(5)	3419(3)	53.2(16)
C4CA	6850(6)	7967(5)	1941(3)	54.7(16)
C5CA	-409(6)	3644(5)	1117(4)	54.7(16)
O9	-56(8)	1250(6)	5203(3)	132(3)
C1AA	677(6)	2091(6)	860(4)	64(2)
C3AA	-11(6)	2123(5)	1385(4)	58.1(18)
C4AA	2629(6)	1231(5)	1660(3)	54.6(16)
C5AA	2781(6)	6926(5)	4010(3)	56.2(17)
C19	-642(6)	5565(5)	2483(4)	56.4(17)
C22	2454(6)	1666(5)	1123(4)	59.6(18)
C8AA	9(6)	6388(6)	3008(4)	58.9(17)
C0BA	749(6)	6245(6)	1747(4)	60.4(18)
C28	1051(6)	7141(5)	2907(4)	54.6(17)
C3BA	2157(11)	6728(11)	967(6)	174(7)
C4BA	2609(6)	5330(7)	4756(4)	79(2)
C33	1833(6)	7988(5)	3485(4)	64.5(19)
C6BA	5211(11)	4197(8)	656(5)	130(4)
N7BA	6602(7)	1103(6)	23(4)	100(2)
C41	-969(6)	4505(5)	1277(3)	57.3(17)
C1CA	792(6)	2817(7)	446(4)	68(2)
C2CA	1381(6)	7047(5)	2255(4)	63.6(19)
C3CA	1283(6)	1255(6)	713(4)	72(2)
C49	252(7)	3583(6)	581(4)	65.2(19)
C52	-1032(7)	5585(7)	3865(4)	87(3)
C53	3371(6)	2472(5)	954(3)	60.4(19)

C56	1792(8)	19(8)	2373(5)	105(3)
C58	6256(10)	8051(8)	1322(4)	86(3)
C59	4961(8)	9350(6)	2699(5)	83(2)
C62	1201(8)	4349(7)	2974(5)	81(2)
C69	2726(10)	4840(11)	2267(6)	145(5)
C72	7566(11)	779(10)	-44(6)	141(5)
C74	2531(15)	3476(12)	2942(6)	192(8)
C77	5530(30)	851(14)	-445(12)	380(30)
O80	5410(20)	1588(18)	-193(11)	317(10)
C9CA	-877(6)	-270(6)	3335(4)	62.2(18)
C8CA	6560(12)	1545(12)	723(8)	209(9)
C3	1251(16)	3005(18)	-646(8)	223(10)

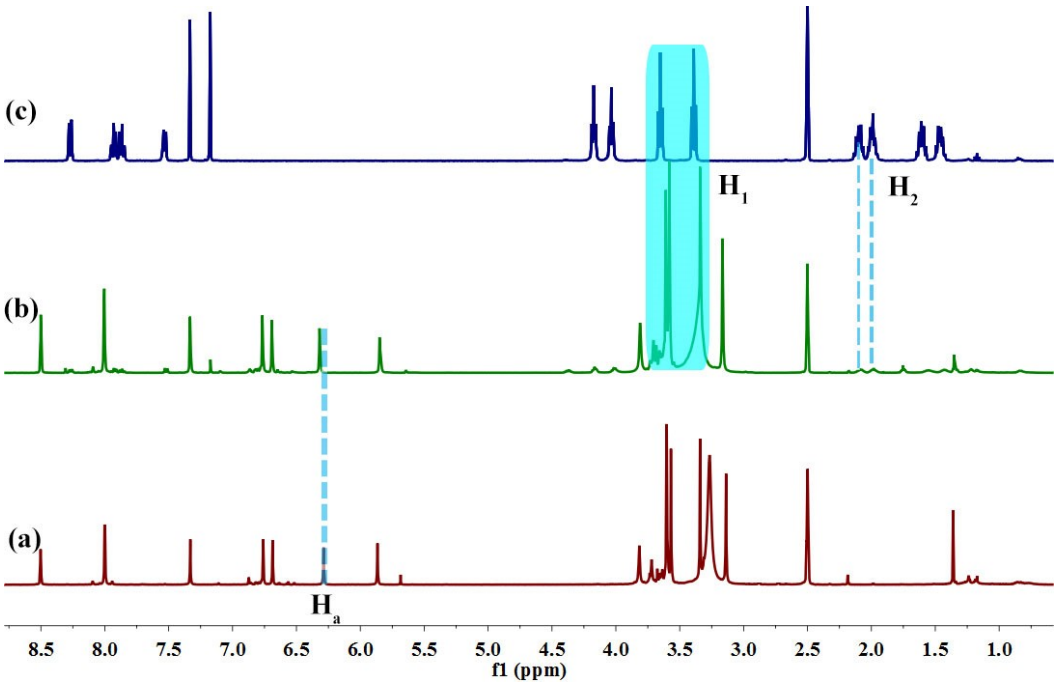

Figure S12 Partial spectra of ^{1}H NMR (400 MHz, DMSO-d_6, 298K) of EYB upon complexation with 2.0 equiv. of Zn(II)TCP (5 mg/mL); (a) Zn(II)TCP; (b) Zn(II)TCP⊃EYB; (c) EYB.

^{1}H NMR titration results showed that the peaks of the alkyl protons H_1 and H_2 in the EYB had a large shift to the upfield (Δδ= -0.12 and -0.21 ppm, respectively) because of the shielding effect of the pillar[5]arene with electron-rich cavities, while the phenyl proton Ha from Zn(II)TCP moved downfield.

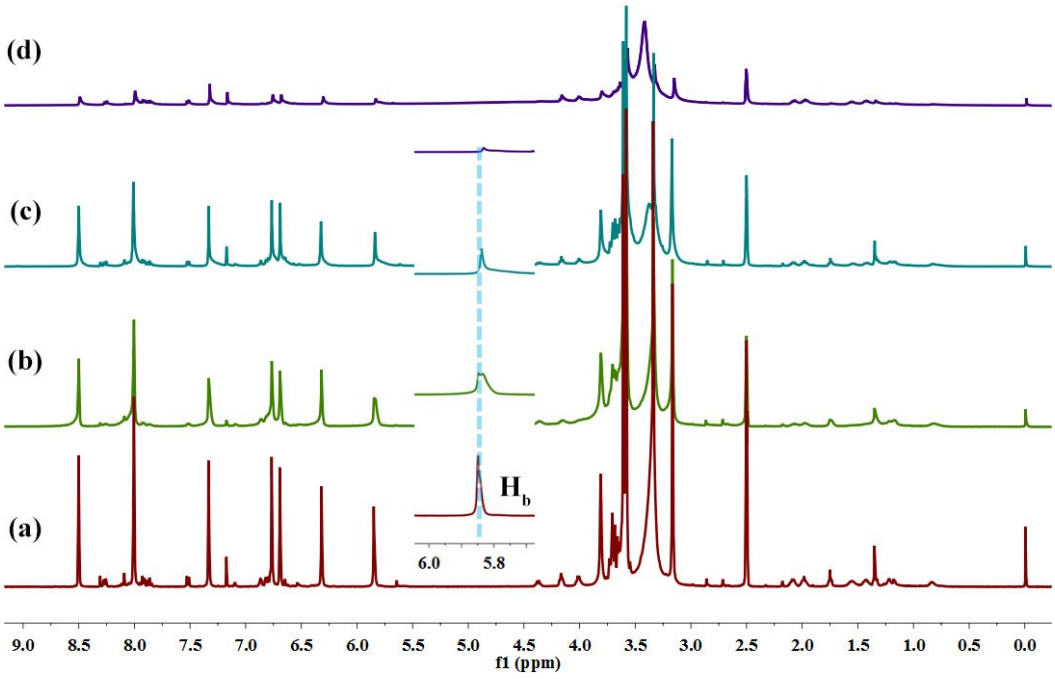

Figure S13 Partial spectra of ^{1}H NMR (DMSO-d_6, 400 MHz, 298 K) titration of Zn(II)TCP⊃EYB with different equivalents of Pb^{2+}: (a) 0; (b) 0.4; (c) 0.8; (d) 1.2.

The uncoordinated carboxyl group in the Zn(II)TCP further coordinated with the added Pb^{2+} ions, thereby introducing Pb^{2+} ions into the Zn(II)TCP⊃EYB assembly. The ^{1}H NMR titration experiments showed that the signal of the benzene ring proton gradually shifted upfield with the increase of Pb^{2+} concentration, indicating that Pb^{2+} ion coordinated with carboxyl groups.

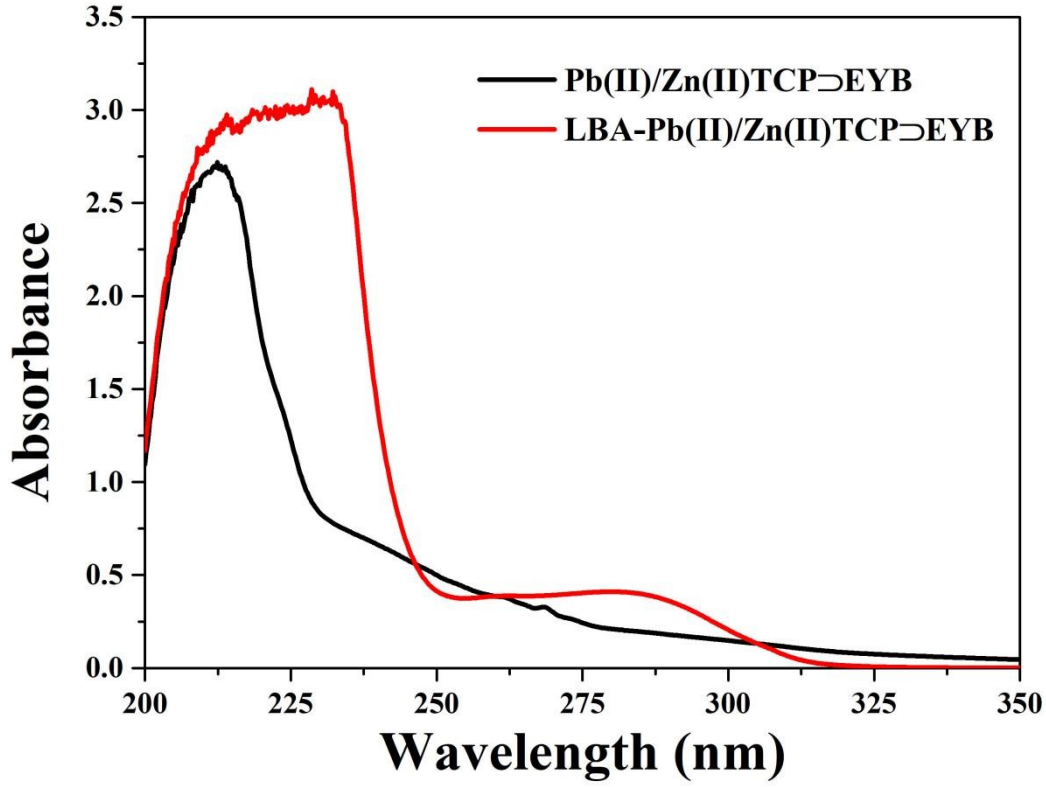

Figure S14 UV/Vis spectrum of Pb(II)/Zn(II)TCP⊃EYB and LBA-Pb(II)/Zn(II)TCP⊃EYB. To achieve the targeted binding of lysozyme of fingerprint ridges, amino-group-labeled LBA (LBA-NH_2) was further modified with Pb(II)/Zn(II)TCP⊃EYB, showed that a typical absorption was observed at 277 nm, indicating the formation of LBA-Pb(II)/Zn(II)TCP⊃EYB.

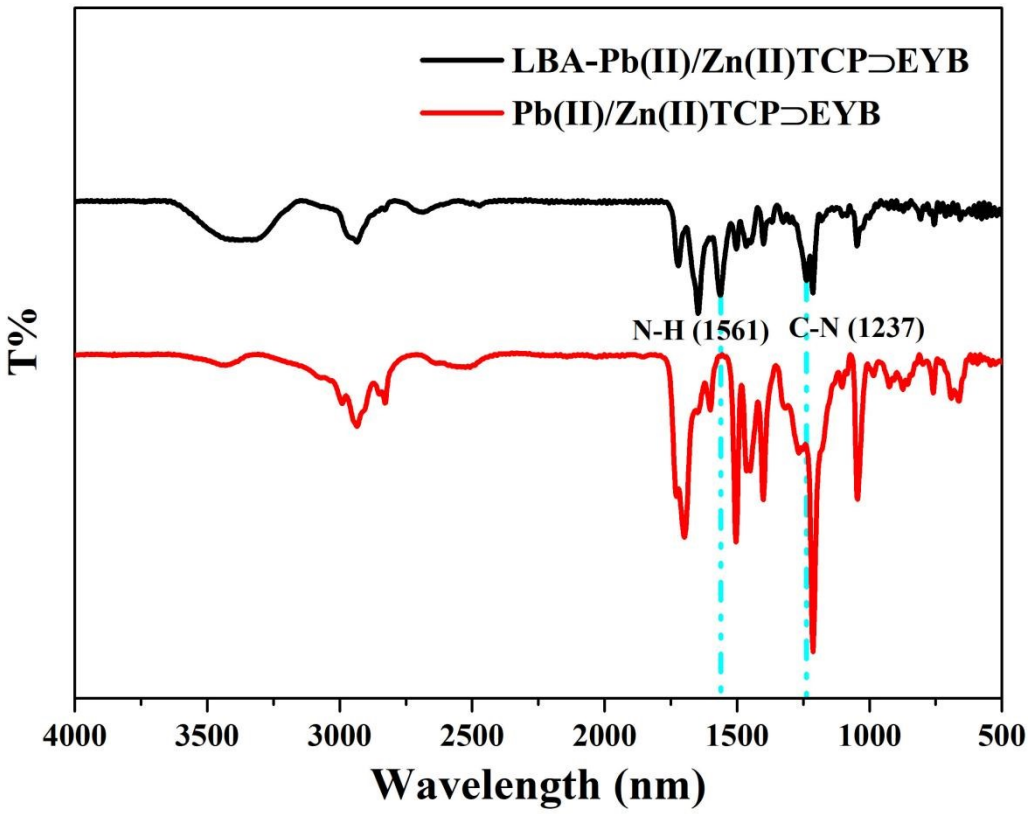

Figure S15 FT-IR spectra of LBA-Pb(II)/Zn(II)TCP⊃EYB and Pb(II)/Zn(II)TCP⊃EYB, the stretching vibration absorption peaks of –C–N and the bending vibration absorption peaks of –N-H– appeared at 1237 and 1561 cm^{-1}, respectively.

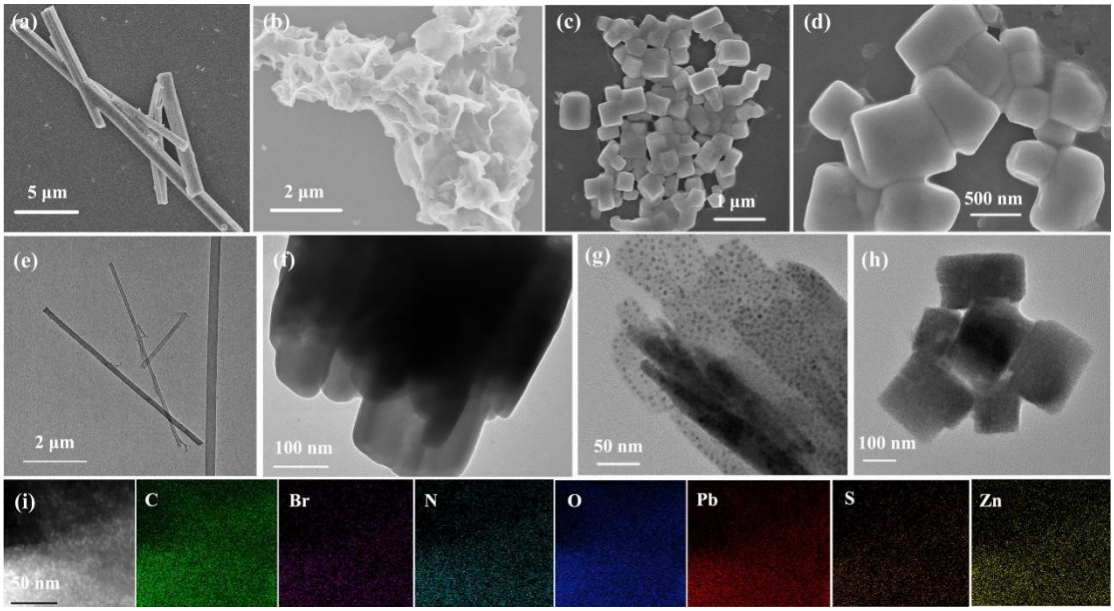

Figure S16 Representative SEM and TEM images showing the morphology of (a) Zn(II)TCP, (b) Zn(II)TCP⊃EYB, (c) $MAPbBr_3$@Zn(II)TCP⊃EYB, (d) $MAPbBr_3$@Zn(II)TCP⊃EYB-NiB; TEM of (e) Zn(II)TCP, (f) Zn(II)TCP⊃EYB, (g) $MAPbBr_3$@Zn(II)TCP⊃EYB, (h) $MAPbBr_3$@ Zn(II)TCP⊃EYB-NiB, and (i) HAADF-STEM image and EDS elemental mappings of different elements of C, N, O, Pb, Br, Zn, and S recorded from $MAPbBr_3$@Zn(II)TCP⊃EYB-NiB.

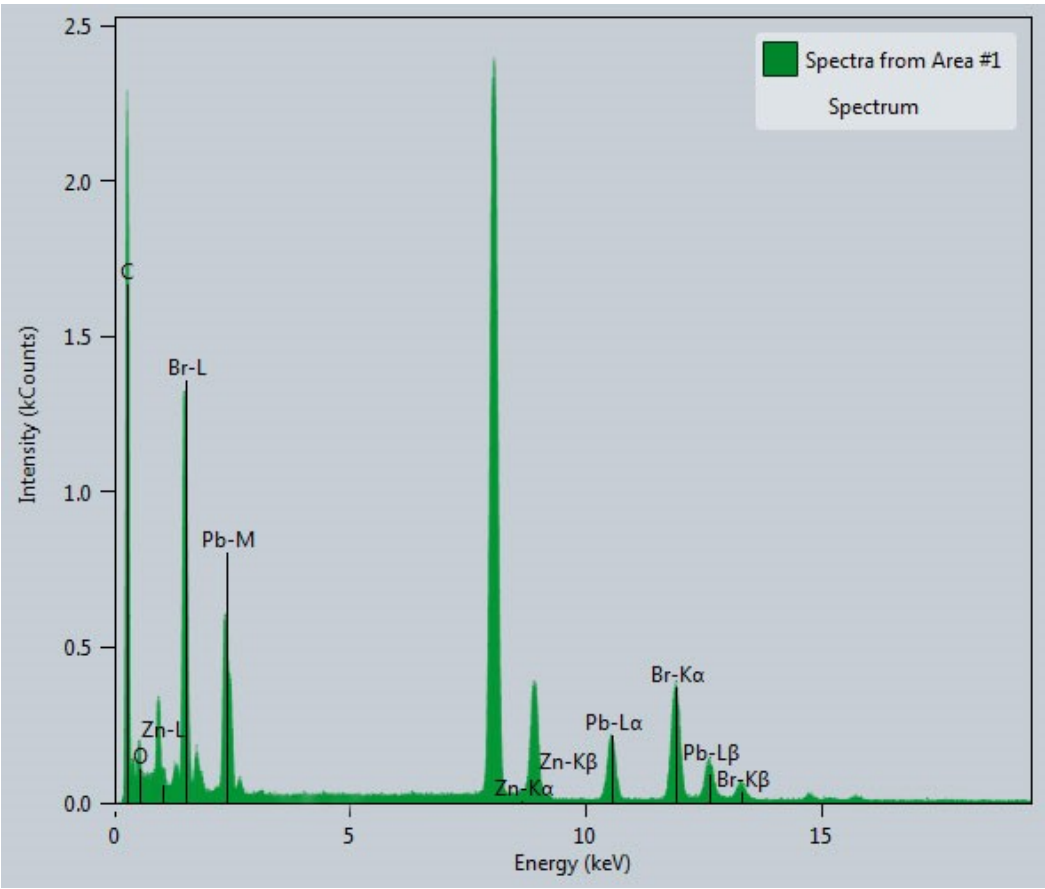

Figure S17 TEM-EDS spectra of $MAPbBr_3$@Zn(II)TCP-EYB.

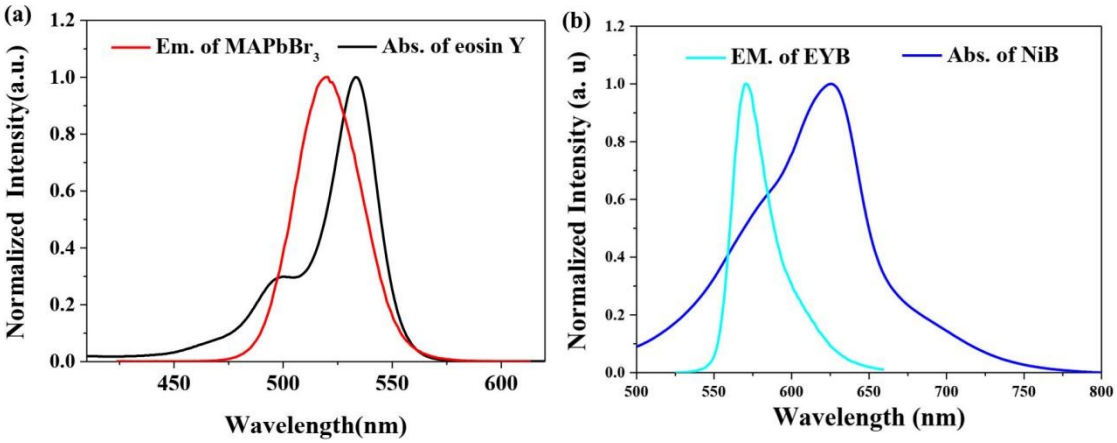

Figure S18 (a) Normalized absorption spectrum of eosin Y and emission spectrum of $MAPbBr_3$, (b) Normalized absorption spectrum of Nile Blue and emission spectrum of $MAPbBr_3$@Zn(II)TCP⊃EYB.

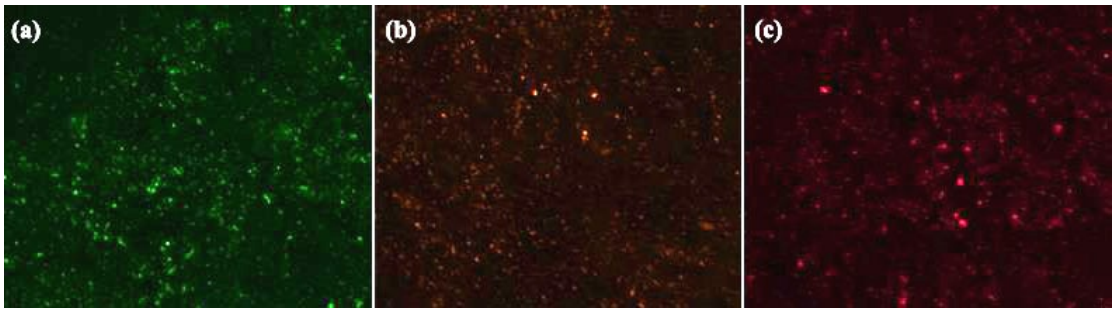

Figure S19 CLSM image of (a) $MAPbBr_3$@Zn(II)TCP, (b) $MAPbBr_3$@Zn(II)TCP⊃EYB and (c) $MAPbBr_3$@Zn(II)TCP⊃EYB-NiB in toluene (λ_{ex}=360 nm).

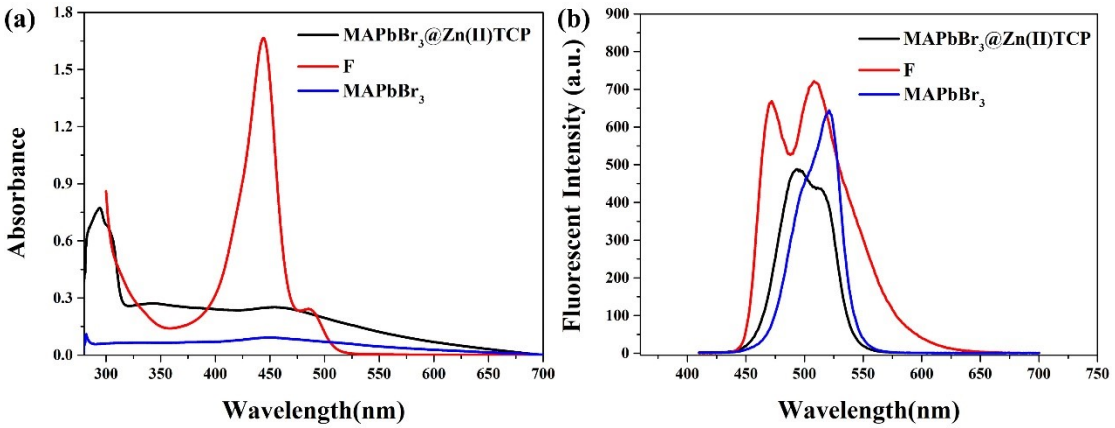

Figure S20 Absorption spectrum of $MAPbBr_3$, $MAPbBr_3$@Zn(II)TCP and Fluorescein; (b) Fluorescence spectra of $MAPbBr_3$, $MAPbBr_3$@Zn(II)TCP and Fluorescein.

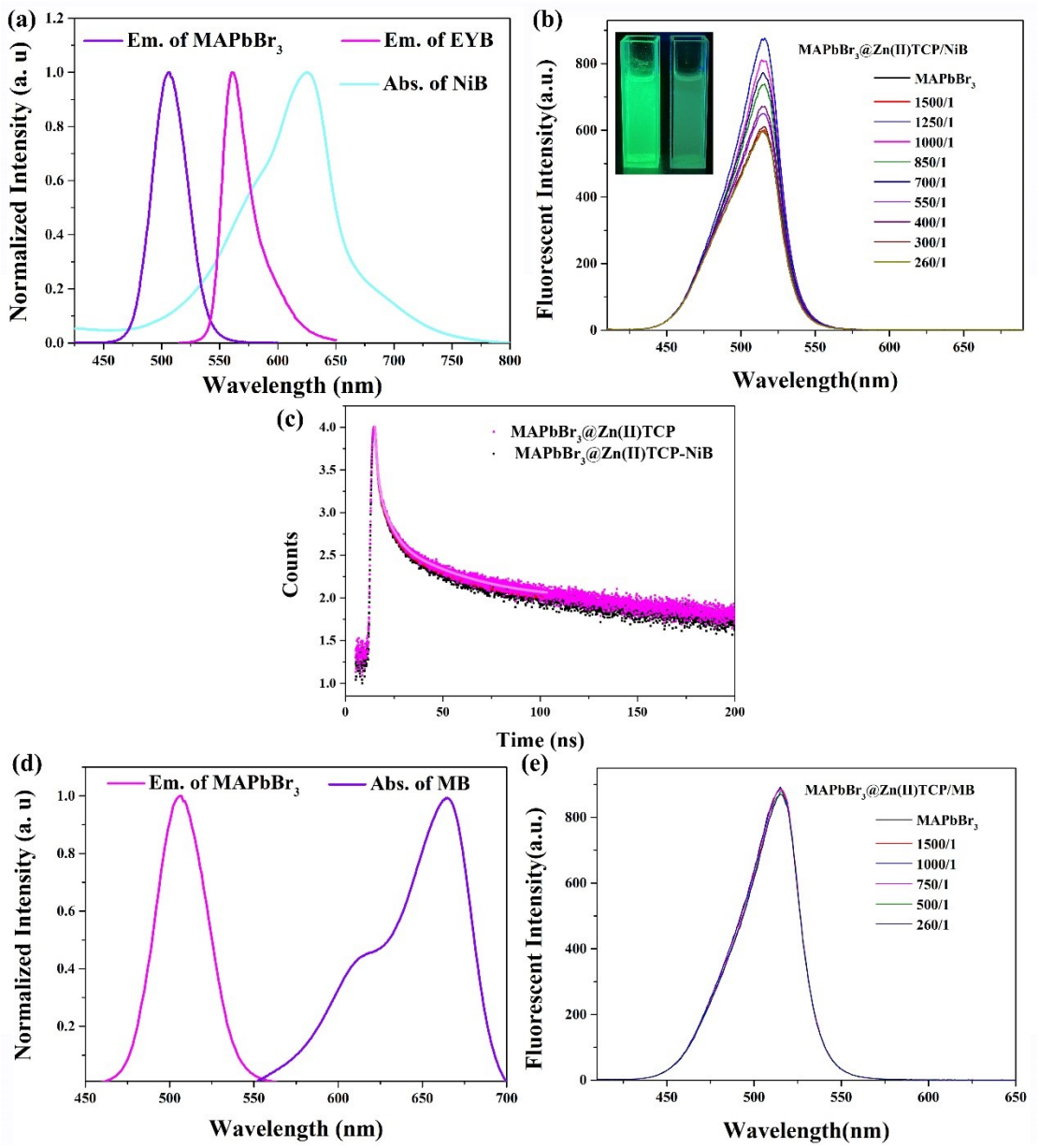

Figure S21 (a) Normalized absorption spectrum of Nile blue and emission spectrum of $MAPbBr_3$, and eosin Y; (b) Fluorescence spectra of $MAPbBr_3$@Zn(II)TCP upon excitation at 360 nm before and after the addition of NiB, inset: fluorescence images of $MAPbBr_3$@Zn(II)TCP (left) and $MAPbBr_3$@Zn(II)TCP-NiB (right); (c) Fluorescence decay profiles of $MAPbBr_3$@Zn(II)TCP and $MAPbBr_3$@Zn(II)TCP-NiB; (d) Normalized absorption spectrum of Methylene Blue (MB) and emission spectrum of $MAPbBr_3$; (e) Fluorescence spectra of $MAPbBr_3$@Zn(II)TCP upon excitation at 360 nm before and after the addition of MB.

In $MAPbBr_3$@Zn(II)TCP-NiB system, the energy transfer efficiency was calculated to be 6.6 % at the donor/acceptor ratio of 260:1 (Figure S21, Table S3), lower than that of $MAPbBr_3$@Zn(II)TCP⊃EYB-NiB system, owing to the less rarely overlap between the absorption spectrum of NiB and the emission spectrum of $MAPbBr_3$ (Figure S21a). In addition, As shown in Figure S21e, with the gradual

addition of MB to $MAPbBr_3$@Zn(II)TCP, the fluorescence intensity of the $MAPbBr_3$@Zn(II)TCP does not change when excited at 360 nm, which is due to no spectral overlap between the absorption band of MB and the emission band of $MAPbBr_3$ QDs.

Table S3. Multiexponential fit parameters for the decay of photoluminescence lifetime at 360 nm.[7]

	τ_1(ns)	B_1	τ_2(ns)	B_2	τ_3(ns)	B_3	average lifetime(ns)
$MAPbBr_3$@Zn(II)TCP	0.63	-801786.4	82.42	7945.09	0.83	803366.8	4.78
$MAPbBr_3$@Zn(II)TCP ⊃EYB	1.10	4121.59	6.20	606.036	1.75	345	1.45
$MAPbBr_3$@Zn(II)TCP ⊃EYB-NiB	0.86	2833	2.23	1345	2.01	4847	1.05

Table S4. Multiexponential fit parameters for the decay of photoluminescence lifetime at 360 nm.[7]

	τ_1(ns)	B_1	τ_2(ns)	B_2	τ_3(ns)	B_3	average lifetime(ns)
$MAPbBr_3$@Zn(II)TCP	9.52	2477.47	39.59	345.18	2.03	6847.97	4.87
$MAPbBr_3$@Zn(II)TCP -NiB	11.76	1831.59	52.67	402.12	1.78	5540.08	4.55

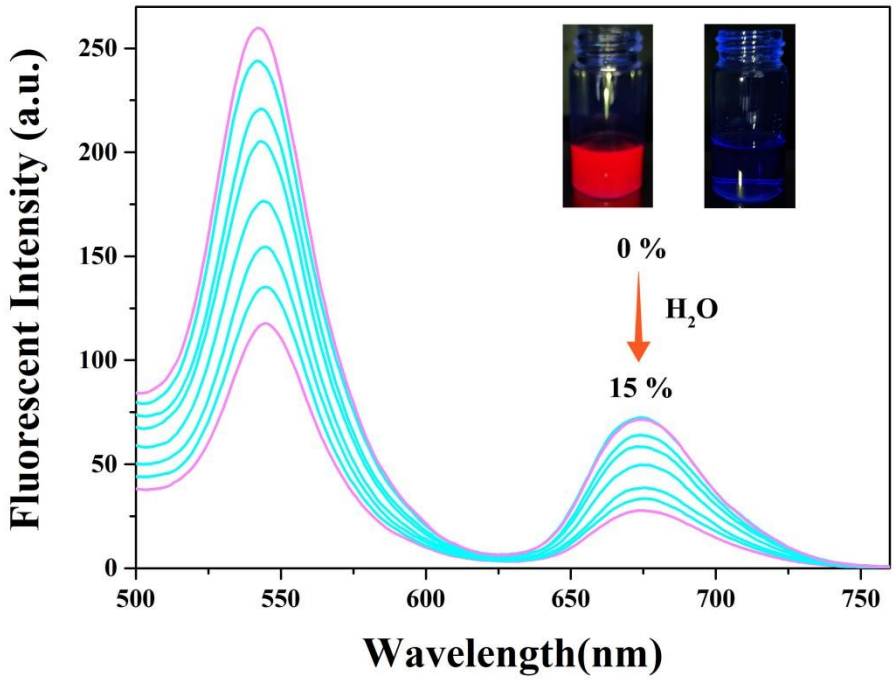

Figure S22 Fluorescence spectra of LBA-MAPbBr$_3$@Zn(II)TCP⊃EYB-NiB with different water fractions in ethanol (λ_{ex}=360 nm).

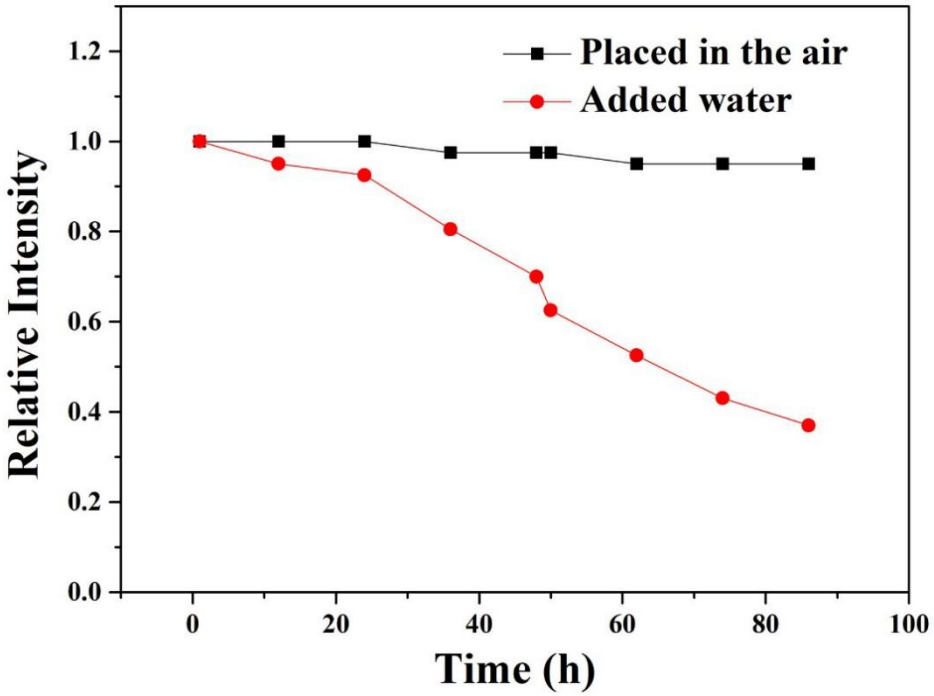

Figure S23 Relative fluorescence intensity of LBA-MAPbBr$_3$@Zn(II)TCP⊃EYB-NiB placed in the air and added water (λ_{ex}=360 nm, λ_{em} =670 nm).

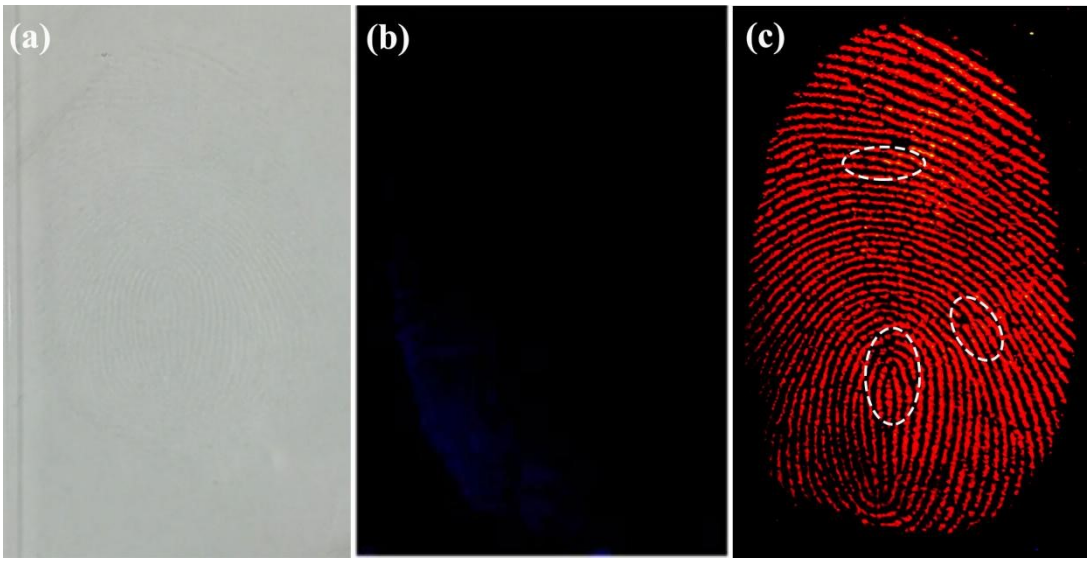

Figure S24 Latent fingerprint on glass slide under (a) natural light and (b) 360 nm light irradiation. (c) Fluorescence image of latent fingerprints labeled by LBA-MAPbBr$_3$@Zn(II)TCP⊃EYB-NiB on the slide.

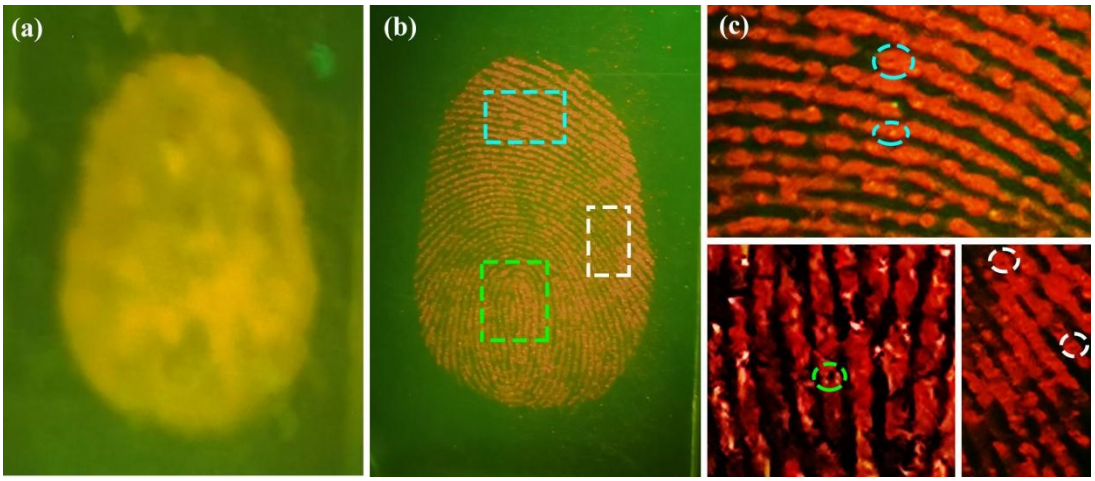

Figure S25 Latent fingerprints imaging experiments. (a) Fluorescence image of latent fingerprints labeled by LBA-MAPbBr$_3$@Zn(II)TCP⊃EYB and (b) LBA-MAPbBr$_3$@Zn(II)TCP⊃EYB-NiB on the blue plastic under 360 nm light irradiation. (c) High-resolution fluorescence images of latent fingerprints showing pore.

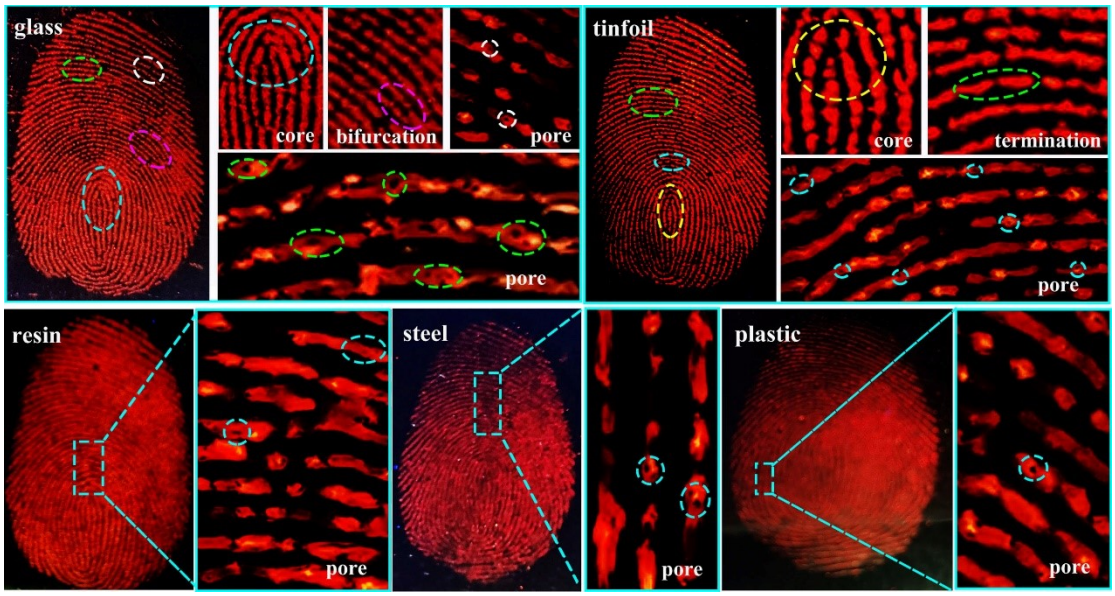

Figure S26 Luminescence image (under 360 nm irradiation) of whole LFPs on different substrates developed by a LBA-$MAPbBr_3$@Zn(II)TCP⊃EYB-NiB solution and Level 1, level 2, and level 3 details of local LFPs on glass, tinfoil, resin, iron and plastic developed by a LBA-$MAPbBr_3$@Zn(II)TCP⊃EYB-NiB solution and the variations of the fluorescence intensity between the fingerprint ridges. Level 1: refers to the overall characteristics of the whole fingerprint, including the shape of the fingerprint (whorl, loop, arch, etc.), the core point (also called the center point), and the triangle point. Level 2 details are the macroscopic detail features of the fingerprint ridge, generally divided into ending, bifurcation, island, and short ridge. Level 3 details are the microscopic detail features of the fingerprint, which mainly include the shape of the ridge edge and the width of the ridge and pore.[8]

References

1. (a) S. B. Wang, B. Y. Guan, X. W. D. Lou, *J. Am. Chem. Soc*. 2018, **140**, 5037−5040. (b) P. J. Yang, P. J. Ou, Y. X. Fang, X. C. Wang, *Angew. Chem. Int. Ed.* 2017, **56**, 3992−3996.
2. (a) J. Ye, M. M. Byranvand, C. O. Martinez, R. L. Z. Hoye, M. Saliba, L. Polavarapu, *Angew. Chem. Int. Ed*. 2021, **60**, 2 – 27. (b) L. Xu, J. Li, B. Cai, J. Song, F. Zhang, T. Fang, H. Zeng, *Nat. Commun*. 2020, **11**, 3902. (c) J. Wang, T. Wei, X. Li, B. Zhang, J. Wang, C. Huang, Q. Yuan, *Angew. Chem. Int. Ed.* 2014, **53**, 1616-1620. (d) M. Famulok, G. Mayer, A. M. Blind, *Acc. Chem. Res*. 2000, **33**, 591-599.
3. (a) Z. Li, X. Li, Y. W. Yang, *Small.* 2019, **15**, 1805509. (b) S. N. Talapaneni, D. Kim, G. Barin, O. Buyukcakir, S. H. Je, A. Coskun, *Chem. Mater.* 2016, **28**, 4460-4466. (c) X. L. Wu, Y. Chen, W. J. Hu, Y. A. Liu, X. S. Jia, J. S. Li, B. Jiang, Wen, K. *Org. Biomol. Chem.* 2017, **15**, 4897-4900. (d) N. L. Strutt, D. Fairen-Jimenez, J. Iehl, M. B. Lalonde, R. Q. Snurr, O. K. Farha, J. T. Hupp, J. F. Stoddart, *J. Am. Chem. Soc.* 2012, **134**, 17436-17439.
4. K. Acharyya, S. Bhattacharyya, H. Sepehrpour, S. Chakraborty, S. Lu, B. Shi, X. Li, P. S. Mukherjee, P. J. Stang, *J. Am. Chem. Soc.* 2019, **141**, 14565-14569.
5. (a) K. Rurack, M. Spieles, *Anal. Chem*. 2011, **83**, 1232. (b) J. R. Lakowicz, Principles of Fluorescence Spectroscopy; 3rd ed.; Springer, 2006.
6. (a) J. Hermans, S. Levinson, *J. Opt. Soc. Am*. 1951, **41**, 460. (b) J. N. Demas, G. A. Crosby, Review. *J. Phys. Chem.* 1971, **75**, 991.
7. Z.-J. Li, E. Hofman, J. Li, A. H. Davis, C.-H. Tung, L.-Z. Wu, W. Zheng, *Adv. Funct. Mater.* 2018, **28**, 1704288.
8. Y. L. Wang, C. Li, H. Q. Qu, C. Fan, P. J. Zhao, R. Tian, M. Q. Zhu, *J. Am. Chem. Soc.* 2020, **142**, 7497-7505.